BRNO UNIVERSITY OF TECHNOLOGY

VYSOKÉ UČENÍ TECHNICKÉ V BRNĚ

FACULTY OF ELECTRICAL ENGINEERING AND COMMUNICATION

DEPARTMENT OF RADIO ELECTRONICS

DIGITAL PREDISTORTERS WITH LOW-COMPLEXITY ADAPTATION

ADAPTACE DIGITÁLNÍCH PŘEDZKRESLOVAČŮ S NÍZKOU SLOŽITOSTÍ

SHORTENED VERSION OF DOCTORAL THESIS

ZKRÁCENÁ VERZE DISERTAČNÍ PRÁCE

AUTHOR
AUTOR PRÁCE

Jan Král

ADVISORS
VEDOUCÍ PRÁCE

doc. dr. Ing. Tomáš Götthans
prof. Ing. Roman Maršálek, Ph.D.

BRNO 2022

KEYWORDS

Digital predistortion, power amplifier linearisation, low-complexity predistorter adaptation, feedback undersampling, histogram-based sample selection, comparator-based level-crossing analogue-to-digital converter.

KLÍČOVÁ SLOVA

Digitální předzkreslovač, linearizace výkonových zesilovačů, adaptace předzkreslovače s nízkou složitostí, podvzorkování zpětné vazby, výběr vzorků pomocí histogramu, analogově digitální převodník s detekcí jedné úrovně s komparátorem.

Contents

Introduction

Modern communication systems must provide ever-increasing data throughput. This demand is usually satisfied by increased communication bandwidth and by developing more spectrum-efficient modulation schemes. The modern spectrum-efficient modulations put stringent demands on transmitters and receivers, especially on their hardware imperfections. In the currently developed *fifth generation* (5G) and *sixth generation* (6G) systems, one of the main concerns is the linearity of *radio frequency* (RF) *power amplifiers* (PAs) in transmitters [1], because the nonlinear distortion leads to a degraded constellation diagram resulting in higher bit error rate and to the spectrum regrowth, undesired transmission and potential interference in regions close to the communication channel. The linear PAs, however, suffer from low power efficiency. They are usually physically larger and require powerful cooling systems, which naturally implies their higher manufacturing expenses. Therefore, designers tend to prioritise their power efficiency at the expense of their linearity and overall transmitter linearity is achieved by linearisation techniques.

One of the linearisation techniques is digital predistortion. The *digital predistorter* (DPD) modifies a signal going to the nonlinear PA by artificial nonlinearity with complementary characteristics to cancel the PA nonlinearity. The digital predistortion is currently the most promising linearisation technique with the highest achievable linearisation performance [2]. However, the DPDs, especially their adaptation, are very computationally demanding and often require complex feedback circuits to track changing PA characteristics.

The higher computational and hardware complexity represents one of the current research challenges. Even though a lot of research has been conducted in this direction, e.g. [3–5], there is still plenty of space for improvements. In this thesis, therefore, we have oriented to low-complexity methods for DPDs. The goal of this thesis is to extend state-of-the-art knowledge of low-complexity methods for PA linearisation to make DPDs generally more applicable, less expensive and more efficient. We introduce three key methods to lower the computational and hardware complexity of the DPD adaptation:

- real-valued feedback,
- feedback sample selection,
- feedback with a *level-crossing analogue-to-digital converter* (LC-ADC).

For the conventional PA adaptation, the PA output is usually down converted by an *in-phase and quadrature* (IQ) mixer and both in-phase and quadrature signals are sampled by two *analogue-to-digital converters* (ADCs). The real-valued feedback method enables avoiding one of the two ADCs which reduces the hardware complexity, saves power and lowers transmitter costs.

Usually the feedback ADCs are required to continually sample the PA output at a sampling frequency which covers three to five times of the communication channel bandwidth [6, 7]. The feedback sample selection naturally allows for feedback undersampling, which significantly decreases the power consumption of the feedback ADCs. Additionally, if the feedback samples are carefully selected, only a few samples are required for successful DPD adaptation. Consequently, calculations with lower dimension matrices lead to a significant reduction of computational complexity. Our simulations and analyses show that the computational complexity can be reduced up to 400 times compared with the conventional approach.

The LC-ADC in feedback replaces two conventional feedback ADCs by a simple comparator. The principle of this method is based on combining principles of the real-valued feedback samples and feedback sample selection. The PA output is not continuously sampled and cannot be fully recovered in the digital processing, but rather the comparator detects when the PA output is crossing a set reference voltage. Knowledge of time instants of the comparator output edges and the set reference voltage is sufficient for the DPD adaptation. Our measurements indicate performance of DPD adaptation with the proposed feedback comparable to DPD adaptation with the conventional feedback with two ADCs. The advantages of the LC-ADC are lower power consumption, costs and footprint than of the equivalent feedback solution with conventional ADCs.

The thesis is structured as follows. Chapter 1 introduces theoretical and historical basics of PA linearisation. Mathematical models of PAs and DPDs, signal modulations, and performance metrics, which are used throughout this thesis, are defined here as well. Chapter 2 reviews the recent advances of PA linearisation, especially of the DPDs. We identified several research directions and focused particularly at low-complexity predistortion methods. In Chapter 3, DPD adaptation with real-valued feedback samples by different DPD architectures is described. The linearisation performance of the DPD adapted by the real-valued feedback samples and the conventional approach are simulated and compared. Feedback sample selection methods are analysed in Chapter 4. We present a general principle of sample selection methods for DPD adaptation in different architectures and later we propose various sample selection methods. We analyse their computational complexity reduction and simulated linearisation performance. Additionally, we confirmed the simulation results by measurements. Chapter 5 describes principles of DPD adaptation with the LC-ADC in the feedback, and measurements of its performance on three different hardware setups. Finally, Chapter 6 summarises the proposed low-complexity approaches and discusses their limitations, usability, and advantages.

1 Theoretical Introduction

1.1 Basic Principles of Power Amplifier Linearisation

The basic concepts of linearisation are simple. The transmitted signal or the PA parameters are modified to obtain a desired output signal. Ideally, the predistorter is set to cancel out the distortion of the transmitter nonlinearity. Its characteristics can be seen as a nonlinearity inverse, if the inversion exists. This ideal case is depicted in Fig. 1.1. The concept of the DPD with feedback is shown in Fig. 1.2.
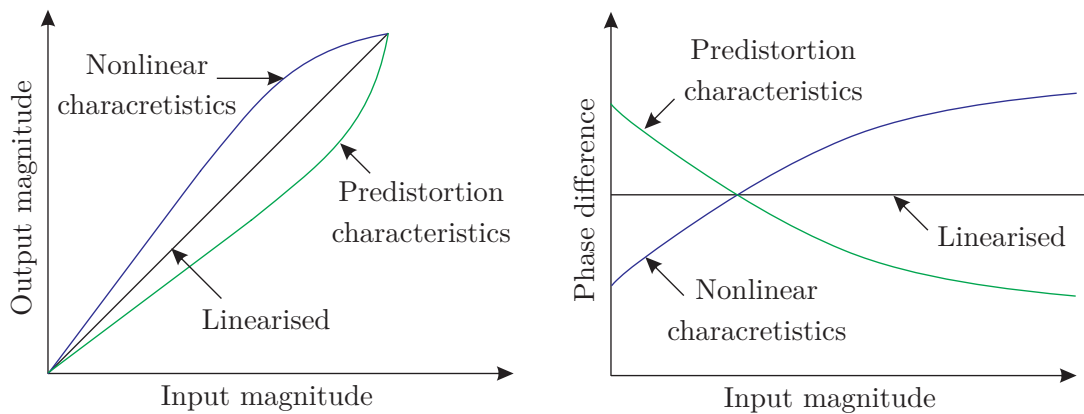
Fig. 1.1: Nonlinearity and ideally-inverted predistortion characteristics in AM/AM and AM/PM plots.
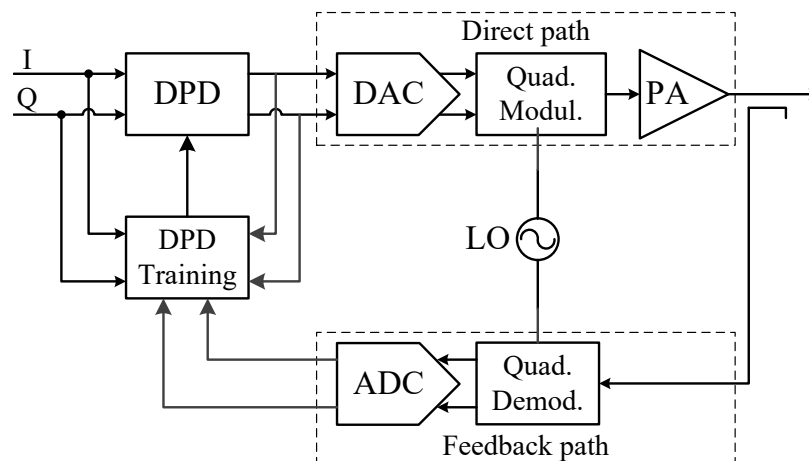
Fig. 1.2: A block diagram of a simplified real system with a digital baseband predistorter.

The motivation behind the predistortion is an increased operating range of amplifiers. The predistortion allows for a reduction in PA back-off and, as the operation moves closer to saturation, an increase in PA efficiency without compromising system linearity. Consequently, the PA dimensions and power rating can be decreased, heat sinks can be miniaturised, and smaller power supplies are required, which naturally results in resource savings and price reduction.

1.2 Employed Models

1.2.1 Memory Polynomial Model

The *memory polynomial* (MP) model is a basic mathematical model for modelling PAs and DPDs [8] The discrete baseband output y of the MP model is given as [8]

$$y[n] = \sum_{k=1}^{K} \sum_{q=0}^{Q} b_{k,q} x[n-q] |x[n-q]|^{k-1}, \tag{1.1}$$

where x is the MP model input, $b_{k,q}$ is the coefficient of the MP model, and K and Q represent the maximum nonlinearity order and memory length, respectively. The product $x[n-q] \, |x[n-q]|^{k-1}$ is often called a basis waveform or a basis function. We denote the basis function as

$$\phi_{k,q}^{(x)}[n] = x[n-q] \, |x[n-q]|^{k-1}. \tag{1.2}$$

The input samples x, model coefficients $b_{k,q}$, and the basis waveforms $\phi_{k,q}^{(x)}[n]$ can be arranged into vectors and matrices

$$
\begin{aligned}
\boldsymbol{\phi}_{k,q}^{(x)} &= \begin{bmatrix} \phi_{k,q}^{(x)}[0] & \phi_{k,q}^{(x)}[1] & \dots & \phi_{k,q}^{(x)}[N-1] \end{bmatrix}^{T}, \\
\boldsymbol{x} &= \begin{bmatrix} x[0] & x[1] & \dots & x[N-1] \end{bmatrix}^{T}, \\
\boldsymbol{y} &= \begin{bmatrix} y[0] & y[1] & \dots & y[N-1] \end{bmatrix}^{T}, \\
\boldsymbol{b} &= \begin{bmatrix} b_{1,0} & b_{1,1} & \dots & b_{1,Q} & b_{2,0} & \dots & b_{K,Q} \end{bmatrix}^{T}, \\
\boldsymbol{U}_x &= \begin{bmatrix} \boldsymbol{\phi}_{1,0}^{(x)} & \boldsymbol{\phi}_{1,1}^{(x)} & \dots & \boldsymbol{\phi}_{1,Q}^{(x)} & \boldsymbol{\phi}_{2,0}^{(x)} & \dots & \boldsymbol{\phi}_{K,Q}^{(x)} \end{bmatrix}^{T},
\end{aligned}
\tag{1.3}
$$

where $\boldsymbol{b}$ is a column vector with $P = K(Q+1)$ rows, and the size of the matrix $\boldsymbol{U}_x$ is $N \times K(Q+1)$. Equation (1.1) can be rewritten into the matrix form

$$\boldsymbol{y} = \boldsymbol{U}_x \boldsymbol{b}. \tag{1.4}$$

1.2.2 Simplified 2nd-Order Dynamic Deviation Reduction-Based Volterra Model

The *simplified 2nd-order dynamic deviation reduction-based Volterra* (DDR2) model has been defined as [9]

$$
\begin{aligned}
y[n] = & \sum_{k=0}^{\frac{K-1}{2}} \sum_{q=0}^{Q} b_{0,k,q} \, |x[n]|^{2k} \, x[n-q] + \\
& + \sum_{k=1}^{\frac{K-1}{2}} \sum_{q=1}^{Q} b_{1,k,q} \, |x[n]|^{2(k-1)} \, x^2[n] \, x^*[n-q] + \\
& + \sum_{k=1}^{\frac{K-1}{2}} \sum_{q=1}^{Q} b_{2,k,q} \, |x[n]|^{2(k-1)} \, x[n] \, |x[n-q]|^2 + \\
& + \sum_{k=1}^{\frac{K-1}{2}} \sum_{q=1}^{Q} b_{3,k,q} \, |x[n]|^{2(k-1)} \, x^*[n] \, x^2[n-q],
\end{aligned}
\tag{1.5}
$$

where $b_{0,k,q}$, $b_{1,k,q}$, $b_{2,k,q}$, $b_{3,k,q}$ are the model coefficients. We can denote the basis function as

$$
\phi_{i,k,q}^{(x)}[n] = \begin{cases}
|x[n]|^{2k} \, x[n-q] & \text{if } i = 0, \\
|x[n]|^{2(k-1)} \, x^2[n] \, x^*[n-q] & \text{if } i = 1, \\
|x[n]|^{2(k-1)} \, x[n] \, |x[n-q]|^2 & \text{if } i = 2, \\
|x[n]|^{2(k-1)} \, x^*[n] \, x^2[n-q] & \text{if } i = 3.
\end{cases}
\tag{1.6}
$$

The model coefficients $b_{i,k,q}$ and the basis waveforms $\phi_{k,q}[n]$ can be arranged into vectors and a matrix similarly as in (1.3)

$$
\begin{aligned}
\boldsymbol{\phi}_{i,k,q}^{(x)} &= \begin{bmatrix} \phi_{i,k,q}^{(x)}[0] & \phi_{i,k,q}^{(x)}[1] & \cdots & \phi_{i,k,q}^{(x)}[N-1] \end{bmatrix}^T, \\
\boldsymbol{b} &= \begin{bmatrix} b_{0,1,0} & b_{0,1,1} & \cdots & b_{0,1,Q} & b_{0,2,0} & \cdots & b_{3,K,Q} \end{bmatrix}^T, \\
\boldsymbol{U}_x &= \begin{bmatrix} \boldsymbol{\phi}_{0,1,0}^{(x)} & \boldsymbol{\phi}_{0,1,1}^{(x)} & \cdots & \boldsymbol{\phi}_{0,1,Q}^{(x)} & \boldsymbol{\phi}_{0,2,0}^{(x)} & \cdots & \boldsymbol{\phi}_{3,K,Q}^{(x)} \end{bmatrix}^T,
\end{aligned}
\tag{1.7}
$$

where $\boldsymbol{b}$ is a column vector with $P = K(2Q + \frac{1}{2}) - Q + \frac{1}{2}$ rows, and the size of the matrix $\boldsymbol{U}_x$ is $N \times K(2Q + \frac{1}{2}) - Q + \frac{1}{2}$. The matrix form of the model equation is the same as (1.4).

1.3 DPD Adaptation Strategies

1.3.1 Direct Learning Architecture

A typical approach to obtaining the solution is based on solving the nonlinear function numerically using Newton's method. Let us assume that the predistortion function is prescribed by equation (1.4). Throughout the thesis, the iterative damped

Newton's method is employed to solve the DPD coefficients. The coefficients are updated as [10]

$$\hat{\boldsymbol{b}} = \boldsymbol{b}' - \mu \boldsymbol{e}, \tag{1.8}$$

where vectors $\hat{\boldsymbol{b}}$, $\boldsymbol{b}'$ are new and current solution of the DPD coefficients, μ is the iteration step size, and vector $\boldsymbol{e}$ is the coefficient error vector. It is given as the *least squares* (LS) solution of

$$\boldsymbol{\Delta} \approx \boldsymbol{U}_z \boldsymbol{e}, \tag{1.9}$$

where $\boldsymbol{\Delta} = \boldsymbol{z} - \boldsymbol{y}$. The solution of $\boldsymbol{e}$ with a pseudoinverse of matrix $\boldsymbol{U}_z$ can be written as

$$\boldsymbol{e} = (\boldsymbol{U}_z^H \boldsymbol{U}_z)^{-1} \boldsymbol{U}_z^H \boldsymbol{\Delta}. \tag{1.10}$$

The final equation of the coefficient update is given by incorporating equation (1.10) into (1.8) as

$$\hat{\boldsymbol{b}} = \boldsymbol{b}' - \mu (\boldsymbol{U}_z^H \boldsymbol{U}_z)^{-1} \boldsymbol{U}_z^H (\boldsymbol{z} - \boldsymbol{y}). \tag{1.11}$$

1.3.2 Indirect Learning Architecture

The *indirect learning architecture* (ILA) solves the postdistorter instead of the predistorter. The solution of the postdistorter is given by linear algebra as

$$\boldsymbol{b}' = (\boldsymbol{U}_y^H \boldsymbol{U}_y)^{-1} \boldsymbol{U}_y^H \boldsymbol{x}, \tag{1.12}$$

where $(\boldsymbol{U}_y^H \boldsymbol{U}_y)^{-1} \boldsymbol{U}_y^H$ is a pseudoinverse of matrix $\boldsymbol{U}_y$. The postdistorter coefficients are used for the predistorter.

2 State-of-the-Art

In recent publications in the field of predistortion, we have identified the following research directions: adaptation methods, analogue and hybrid predistorters, analysis, antenna arrays and *multiple-input and multiple-output* (MIMO) systems, Doherty power amplifiers, hardware implementation, low-complexity methods, machine learning, mathematical models.

Furthermore, the papers about low-complexity predistortion can be divided based on their focus: computational complexity, model pruning and sizing, one-bit feedback samples, real-valued feedback samples, subband and multiband predistortion, and undersampling methods.

2.1 Real-Valued Feedback Samples

Chani-Cahuana et al. [3] proposed a DPD architecture with real-valued feedback samples. They estimated the PA forward model similarly to the procedure described in Sec. 3.2. Afterwards, they employed the same procedure for the *iterative learning control* (ILC)-based DPD adaptation, originally described in [11]. The authors reported the same linearisation performance of the proposed ILC with real-valued feedback samples as that of the original ILC DPD.

Guan et al. [5] presented a *direct learning architecture* (DLA) DPD with one undersampling ADC in the feedback path. Basically, they proposed the same idea as Chani-Cahuana et al. in [3], but employed the DLA instead of the ILC and added undersampling. Both papers seem to be independent. Guan et al. reported, quite surprisingly, a higher linearisation performance of their real-valued undersampled DLA DPD than that of the conventional full-speed complex-valued DPD.

Zhang et al. [12] derived the same formula as Guan et al. [5] in a little different way and without the undersampling.

2.2 One-Bit and Signed-Based Feedback Samples

Wang et al. [4, 13] proposed DPD adaptation based on observing the sign of the PA output error signal. They observed the sign employing the comparators in the feedback path and, in principle, these comparators could be understood as 1-bit ADCs. The simplified diagram of their DPD architecture is depicted in Fig. 2.1.

Pascual Campo et al. [15] presented a comprehensive overview of sign-based algorithms for DPD adaptation. The authors compared the complexities and performance of individual algorithms as well as combinations of them.
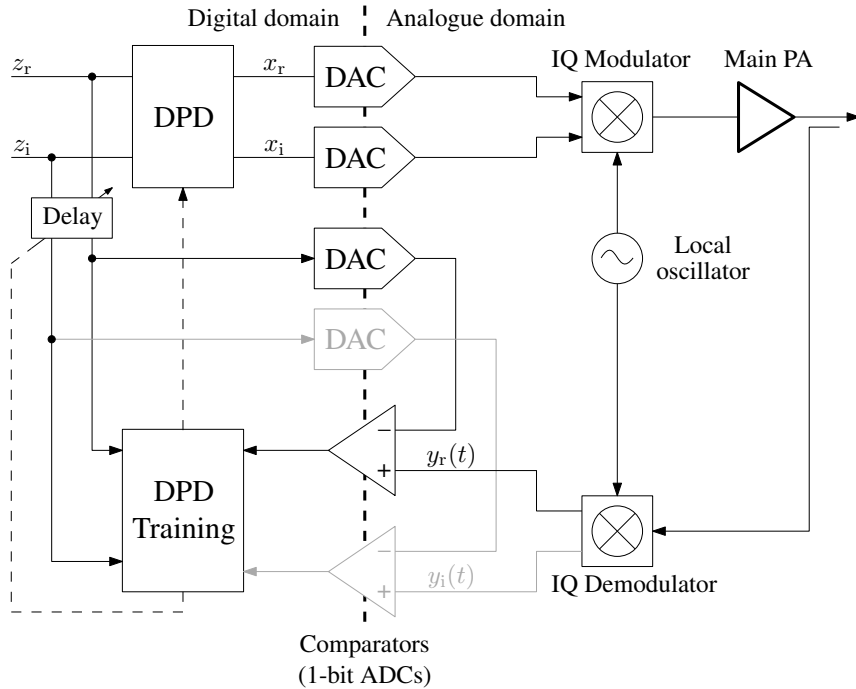
Fig. 2.1: The simplified DPD architecture with comparators in the feedback path as proposed by Wang et al. in [4, 13]. Grey-coloured parts are not required if real-valued feedback principle [14] is employed.

2.3 Undersampling Methods

Huang et al. [16] proposed the DPD adaptation with undersampled feedback. They employed the DLA and kept every n-th feedback sample. They noted that the feedback must be sampled with sufficient bandwidth.

Prata et al. [17] presented feedback loops employing RF subsampling ADCs to improve concurrent dual-band transmitter linearisation. The aliasing between upper and lower bands could naturally occur which the authors compensated for based on statistical approximated nonoverlapped multisines. The authors reported similar performance to the other subsampling techniques but with a lower hardware complexity.

Li et al. [18] focused on time-interleaved DPDs to reduce their sampling rates. The authors proposed a few architectures with time-interleaved DPDs and solved the aliasing effect. Their proposed low-speed DPD was naturally narrow band and compensated only for the distortion close to the communication band. In that region, the authors reported performance similar to that of the full high-speed DPDs.

3 Real-Valued Feedback

3.1 Introduction

In this chapter, we describe a simplification of the feedback circuitry for the DPD adaptation by employing only the in-phase or quadrature output of the IQ down-converting mixer. The in-phase feedback is depicted in a block diagram in Fig. 3.1. The main motivation is to avoid one feedback ADC, which is one of the main contributors to the total system power consumption. Our contribution has been presented in the paper [A3] and is the natural evolution of methods described by Chani-Cahuana et al. in [3] and by Guan et al. in [5].
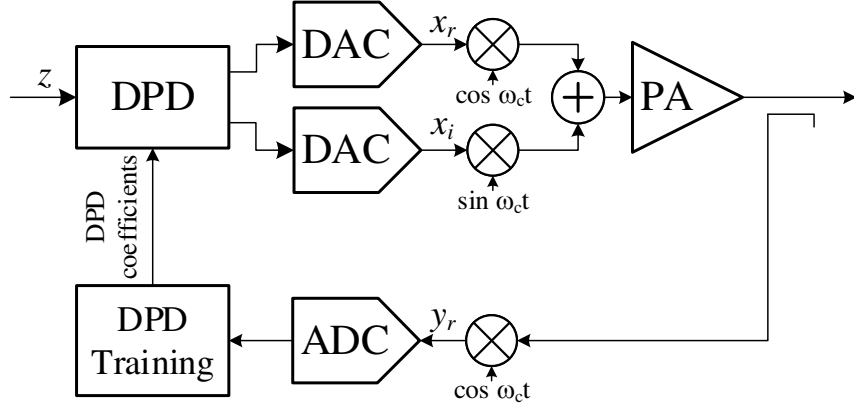

Fig. 3.1: The system diagram for the DPD with real-valued feedback.

3.2 Forward Model Estimation

For simplicity, we start our derivation of the real-valued feedback with the MP model. We can rewrite equation (1.4) with the real and imaginary parts, denoted as $(\cdot)_\mathrm{r}$ and $(\cdot)_\mathrm{i}$, respectively, as

$$\boldsymbol{y}_\mathrm{r} + j\boldsymbol{y}_\mathrm{i} = (\boldsymbol{U}_{x\mathrm{r}} + j\boldsymbol{U}_{x\mathrm{i}})(\boldsymbol{b}_\mathrm{r} + j\boldsymbol{b}_\mathrm{i}). \tag{3.1}$$

Expanding the multiplication on the right-hand side yields

$$\boldsymbol{y}_\mathrm{r} + j\boldsymbol{y}_\mathrm{i} = \boldsymbol{U}_{x\mathrm{r}}\boldsymbol{b}_\mathrm{r} + j\boldsymbol{U}_{x\mathrm{i}}\boldsymbol{b}_\mathrm{r} + j\boldsymbol{U}_{x\mathrm{r}}\boldsymbol{b}_\mathrm{i} - \boldsymbol{U}_{x\mathrm{i}}\boldsymbol{b}_\mathrm{i}, \tag{3.2}$$

which can be split into two systems of equations, one for the real part of $\boldsymbol{y}$ and the other one for the imaginary part of $\boldsymbol{y}$

$$\boldsymbol{y}_\mathrm{r} = \boldsymbol{U}_{x\mathrm{r}}\boldsymbol{b}_\mathrm{r} - \boldsymbol{U}_{x\mathrm{i}}\boldsymbol{b}_\mathrm{i} \quad \wedge \quad \boldsymbol{y}_\mathrm{i} = \boldsymbol{U}_{x\mathrm{i}}\boldsymbol{b}_\mathrm{r} + \boldsymbol{U}_{x\mathrm{r}}\boldsymbol{b}_\mathrm{i}. \tag{3.3}$$

To obtain the PA coefficient vector $\boldsymbol{b}$, it is sufficient to solve only one of the two systems of equations. Matrix $\boldsymbol{U}_x$ is fully known, as it consists of samples given by the transmitted signal x. Therefore, we can obtain $\boldsymbol{b}$ as the LS solution with the real feedback samples

$$\begin{bmatrix} \boldsymbol{b}_\mathrm{r} \\ \boldsymbol{b}_\mathrm{i} \end{bmatrix} = (\boldsymbol{A}_x^H \boldsymbol{A}_x)^{-1} \boldsymbol{A}_x^H \boldsymbol{y}_\mathrm{r}, \tag{3.4}$$

where we have substituted $\boldsymbol{A}_x = \begin{bmatrix} \boldsymbol{U}_{x\mathrm{r}} & -\boldsymbol{U}_{x\mathrm{i}} \end{bmatrix}$.

3.3 Indirect Learning Architecture

Direct derivation of the ILA with real-valued feedback cannot be achieved. However, we can benefit from [19, 20] and employ the *forward model indirect learning architecture* (FM-ILA) with real-valued feedback. Hereinafter, we will refer to the proposed method as the *real-valued forward-model indirect learning architecture* (R-FM-ILA).

3.4 Direct Learning Architecture

The solution for the updated DPD coefficients can be obtained similarly as

$$\begin{bmatrix} \hat{\boldsymbol{b}}_r \\ \hat{\boldsymbol{b}}_i \end{bmatrix} = \begin{bmatrix} \boldsymbol{b}'_r \\ \boldsymbol{b}'_i \end{bmatrix} - \mu(\boldsymbol{A}_z^H \boldsymbol{A}_z)^{-1} \boldsymbol{A}_z^H (\boldsymbol{z}_r - \boldsymbol{y}_r). \tag{3.5}$$

Hereinafter, the DLA with real feedback samples is referred to as the *real-valued direct learning architecture* (R-DLA).

3.5 Simulation

We have implemented and simulated DPD architectures with real-valued feedback (R-DLA, R-FM-ILA) to evaluate their linearisation performance. We have performed simulations for conventional architectures with complex feedback (ILA, DLA, FM-ILA) and for the system without the DPD to compare all of them with the recently introduced R-FM-ILA and R-DLA.

The linearisation performance has been evaluated based on the *normalised mean square error* (NMSE) and *adjacent channel power ratio* (ACPR). We have simulated all architectures with the DPD modelled by the MP model with the maximum nonlinearity order of $K = 7$ and the maximum memory length of $Q = 3$. In the simulation, all the architectures have been computed with 220 iterations. The evaluated metrics were averaged over the last 200 iterations, which corresponds to the range where the DLA and R-DLA converged.

The frequency spectra of the PA output are shown in Fig. 3.2. The spectra for all the DPD architectures are almost the same and well improved compared to the spectrum for the system without the DPD.
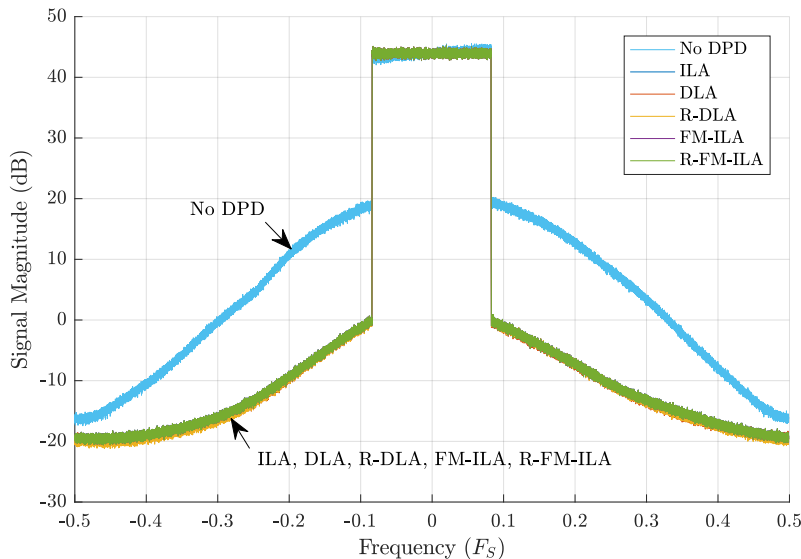

Fig. 3.2: The frequency spectra of the PA output for all simulated architectures. The frequency axis is normalised to the sampling frequency F_s.

The detailed comparison of linearisation performance for all the architectures is given in Tab. 3.1. All the ILA-based systems provide very similar linearisation performance based on the evaluated metrics. The DLA and R-DLA provide very similar results and they are slightly better than the ILA-based systems.

Tab. 3.1: The linearisation performance of systems with real-valued feedback compared with conventional architectures.

DPD architecture	NMSE (dB)	ACPR-1st (dB)	ACPR-2nd (dB)
No DPD	-19.9	-29.6	-46.5
ILA	-40.5	-49.6	-60.3
DLA	-40.8	-49.8	-60.7
R-DLA	-40.7	-49.7	-60.7
FM-ILA	-40.5	-49.6	-60.3
R-FM-ILA	-40.5	-49.6	-60.3

15

4 DPD Adaptation with Sample Selection

4.1 Introduction

In this chapter we propose methods for the selection of samples for DPD adaptation allowing computational complexity reduction. The block diagram for DPD adaptation with sample selection is shown in Fig. 4.1.

The proposed methods are: a method based on the identification of important samples using QR decomposition, a gradient-based sampling method [21], and two histogram-based methods. The first histogram method equalises the histogram of signal magnitudes to ensure evenly sampled PA characteristics while the second one optimises a histogram optimised by a genetic algorithm, which respects both the transmitted signal statistical properties and the specific PA characteristics.

4.2 Basic Principles of Sample Selection

To identify the unknown coefficients $b_{k,q}$ of the PA model, the conventional methods construct a system of equations by taking consecutive input and output baseband
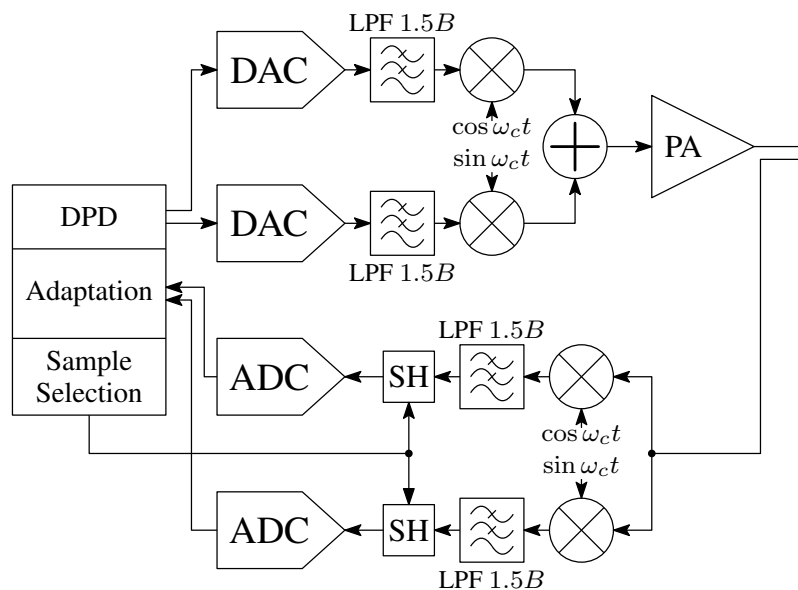

Fig. 4.1: Linearisation of an RF PA with the DPD using a sample selection method. Although the depicted SH circuits as discrete components are one possible approach, a more practical implementation would employ ADCs with integrated SH circuits and with periodic and equidistant sampling, performing sample selection from a sample buffer in the digital domain.

samples of the PA and inserting them into the system of equations (1.4). Practically, to solve the PA model coefficients, the system of equations has to be overdetermined to mitigate the imperfections of the PA input generation and of the PA output measurement. In the overdetermined system, we can eliminate arbitrary rows as

$$
\begin{bmatrix} \cancel{y[0]} \\ y[1] \\ y[2] \\ \cancel{y[3]} \\ \cancel{y[4]} \\ y[5] \\ y[6] \\ y[7] \end{bmatrix} = \begin{bmatrix} \cancel{x[0]} & \cancel{x[-1]} & \cancel{x[0]|x[0]|} & \cancel{x[-1]|x[-1]|} \\ x[1] & x[0] & x[1]|x[1]| & x[0]|x[0]| \\ x[2] & x[1] & x[2]|x[2]| & x[1]|x[1]| \\ \cancel{x[3]} & \cancel{x[2]} & \cancel{x[3]|x[3]|} & \cancel{x[2]|x[2]|} \\ \cancel{x[4]} & \cancel{x[3]} & \cancel{x[4]|x[4]|} & \cancel{x[3]|x[3]|} \\ x[5] & x[4] & x[5]|x[5]| & x[4]|x[4]| \\ x[6] & x[5] & x[6]|x[6]| & x[5]|x[5]| \\ x[7] & x[6] & x[7]|x[7]| & x[6]|x[6]| \end{bmatrix} \begin{bmatrix} b_{0,0} \\ b_{0,1} \\ b_{1,0} \\ b_{1,1} \end{bmatrix}. \tag{4.1}
$$

Advantageously, signal $y[n]$ can be arbitrarily undersampled. This allows for reducing the hardware requirements, e.g., the sampling rate of the feedback ADCs.

Hereinafter, the described method is referred to as the *sample selection method* (SSM). In the following sections, we show some possible ways of employing SSMs in the DPD identification process.

4.3   Sample Selection Methods

The best DPD adaptation can be achieved if the observation errors of the input and output are uncorrelated [22]. However, the adjacent samples used by the conventional DPD are not independent, and therefore the observation errors are correlated. To minimise the observation errors, the conventional methods without sample selection require a high number of samples N, usually $N > 1000$ [22]. For a small N, the subsequent samples cause the system of equations to be ill-conditioned. Furthermore, a limited number of subsequent samples cannot cover the statistical properties of the transmitted signal.

We show that the proposed SSM does not suffer from the mentioned drawbacks for small N if the samples $n_1, n_2, ..., n_N$ are selected carefully. The problem for the sample selection method can be defined as the selection of N samples from all samples which were acquired by the feedback ADCs. The number of all acquired samples is N_0 and corresponds to the acquisition time and hence to the required update rate of DPD coefficients. The number of selected samples is naturally limited by the condition $N \leq N_0$.

4.3.1 Undersampling

A simple undersampling can be seen as an untargeted sample selection and henceforth it is referred to as the *undersampling-based sample selection* (US). Although this method is very simple, it can improve the conditioning of the system of equations and can be sufficient for less demanding applications.

4.3.2 Sample Selection Based on QR Decomposition

The problem of selecting the samples can be solved analytically using QR decomposition with column pivoting [23], hereinafter referred to as *QR-decomposition-based sample selection* (QRS).

4.3.3 Gradient Sampling

Another method for sample selection can be the *gradient-based sampling* (GS) [21], henceforth referred to as *GS-based sample selection* (GSS). GS is a representative of the methods for solving least squares problems of a large sample size.

4.3.4 Histogram-Based SSMs

Samples for DPD adaptation are selected randomly such that the j-th histogram bin count reaches the target bin count d_j, i.e., cardinality $\overline{\overline{D_j}}$ is equal to d_j.

Evenly Distributed Histogram

The motivation for the *evenly distributed histogram* (EDH) is to cover the whole *amplitude/amplitude* (AM/AM) characteristics of PA. Unfortunately, this simple approach of setting target bin counts does not respect either the shape of the AM/AM characteristics of the used PA nor the statistical properties of the transmitted signal which results in a DPD model with similar modelling capabilities in all regions of AM/AM characteristics.

Genetically Optimised Histogram

The *genetically optimised histogram* (GOH) is proposed to suppress EDH imperfections. An optimised histogram can respect the AM/AM characteristics of the PA and the statistics of the transmitted signal, as depicted in Fig. 4.2. We optimise target histogram bin counts by the genetic algorithm to minimise the NMSE.
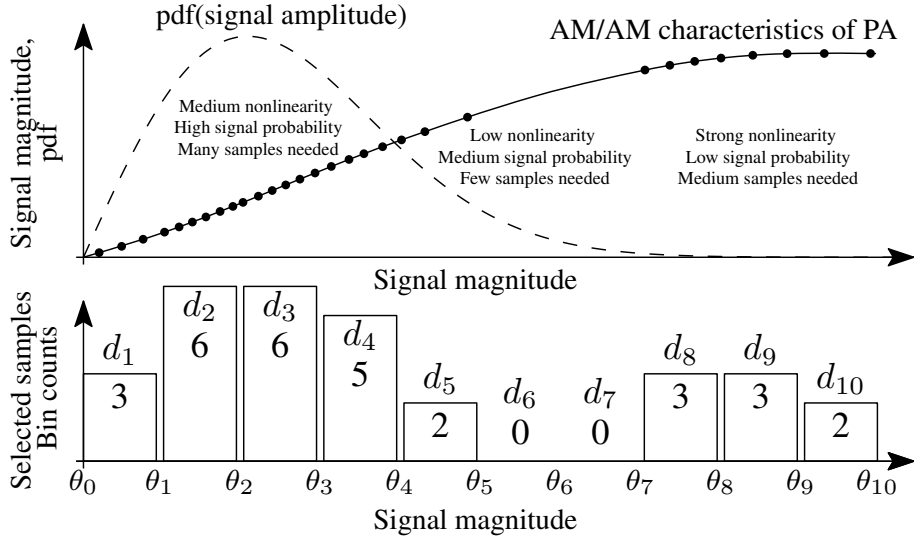
Fig. 4.2: Principle of the sample selection by GOH with $J = 10$ related to the probability density function (pdf) of signal magnitude and the AM/AM characteristics of the PA. The depicted $N = 30$ selected samples are placed in regions with strong nonlinearity and/or high signal probability.

4.4 Reduction of DPD Adaptation Complexity

A few properly selected samples N significantly reduces the computational complexity of DPD adaptation. We evaluate the computational complexity of DPD adaptation with P coefficients and N samples with respect to the required number of real-valued multiplications $O_\otimes(N, P)$ and real-valued additions $O_\oplus(N, P)$.

Tab. 4.1 shows a comparison of the computational complexity. We can conclude that QRS is computationally the most demanding. The least complex methods are histogram-based SSMs whose complexity is the same as for conventional DPD adaptation using a block of continuous feedback samples.

The main advantages of the decreased sampling frequency of the feedback ADCs are the lower power consumption, the decreased system complexity, and the price. Tab. 4.2 gives a comparison of a transmitter with the conventional DPD and a transmitter with the undersampled feedback allowed by the proposed SSM.

4.5 Simulations and Measurements

The proposed methods have been verified by simulations and measurements. The simulated and measured DPD performance in terms of ACPR as a function of number of selected samples N is shown in Fig. 4.3 and Fig. 4.4, respectively. We can

Tab. 4.1: Comparison of Computational Complexity

		Conv. DPD	QRS	GSS	Hist. SSM
$P = 14$	$O_\otimes$	DNC	$3.2 \cdot 10^6$	$3.1 \cdot 10^6$	$22 \cdot 10^3$
$N = 20$	$O_\oplus$	DNC	$2.2 \cdot 10^6$	$2.0 \cdot 10^6$	$26 \cdot 10^3$
$P = 14$	$O_\otimes$	DNC	$3.3 \cdot 10^6$	$3.1 \cdot 10^6$	$62 \cdot 10^3$
$N = 100$	$O_\oplus$	DNC	$2.2 \cdot 10^6$	$2.1 \cdot 10^6$	$74 \cdot 10^3$
$P = 14$	$O_\otimes$	$5.1 \cdot 10^6$	$8.0 \cdot 10^6$	$7.8 \cdot 10^6$	$5.1 \cdot 10^6$
$N = 10^4$	$O_\oplus$	$6.0 \cdot 10^6$	$8.1 \cdot 10^6$	$7.9 \cdot 10^6$	$6.0 \cdot 10^6$

Conventional DPD does not converge (DNC) for a low number of selected samples N. The complexity in the table is calculated for $N_0 = 20\,000$ and the MP model with $K = 7$, and $Q = 1$.

Tab. 4.2: Comparison of System Parameters

	Conventional DPD 2× AD9690	DPD with SSM 2× AD9629
F_S	1000 MSps	20 MSps
Max. B_in	500 MHz	700 MHz
ENOB	10.5 bits	11 bits
Digital interface	JESD204B	Parallel
Power consumption	≈ 4 W	≈ 90 mW
Price	≈ 720 USD	≈ 20 USD

observe that the conventional DPD starts to improve the transmitter linearity when more than 1300 samples are selected. EDH starts to linearise from 19 selected samples and slightly improves with an increasing number of selected samples. In the region of up to $N < 2000$ samples, GOH outperforms all other methods. Please recall that we have 17 DPD coefficients and taking only 18 samples is almost equivalent to solving a fully determined system.

The trend for the measurement results follows the simulation results. For a very small number of selected samples $N = 24$, GOH provides a linearisation performance equivalent to the maximum achievable linearisation performance of the conventional DPD. Since the computational complexity is linear with the number of required samples, this indicates a 400-times complexity reduction over the conventional DPD.
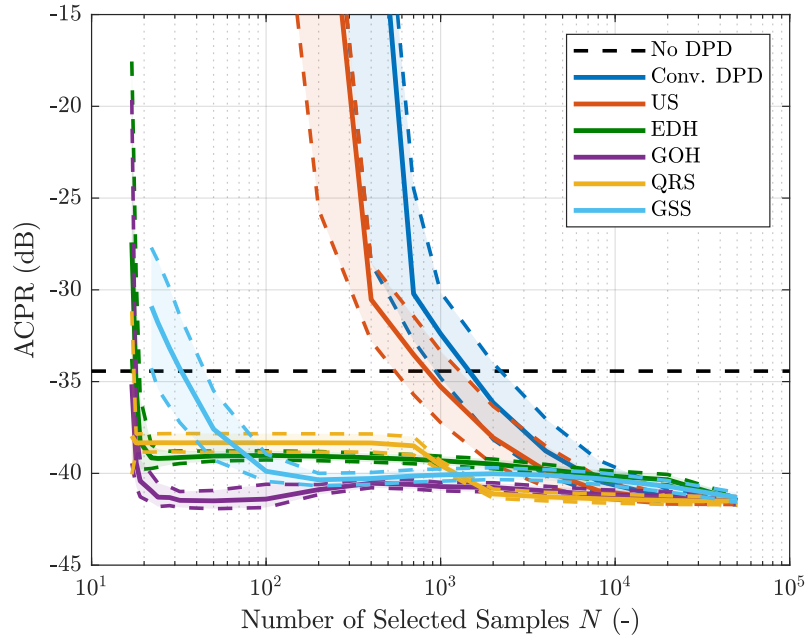
Fig. 4.3: Simulation results of ACPR as a function of the number of selected samples N with 95% confidence intervals depicted by coloured dashed lines for the model PA1. The black dashed line represents the simulated ACPR of the PA output without DPD.
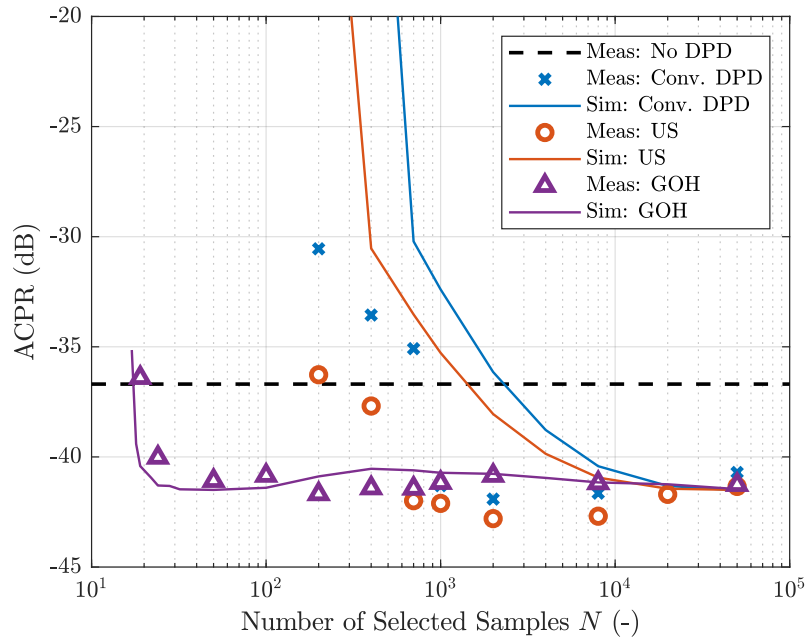

Fig. 4.4: Measurement results of ACPR as a function of the number of selected samples N compared to the simulation results. The black dashed line represents the simulated ACPR of the PA output without DPD.

5 DPD Adaptation with Level-Crossing ADC

5.1 Introduction

We propose a novel method for predistorter adaptation with an LC-ADC based on a comparator and an *low-speed digital-to-analogue converter* (LSDAC) which replaces conventional ADCs in the feedback path (Fig. 5.1).
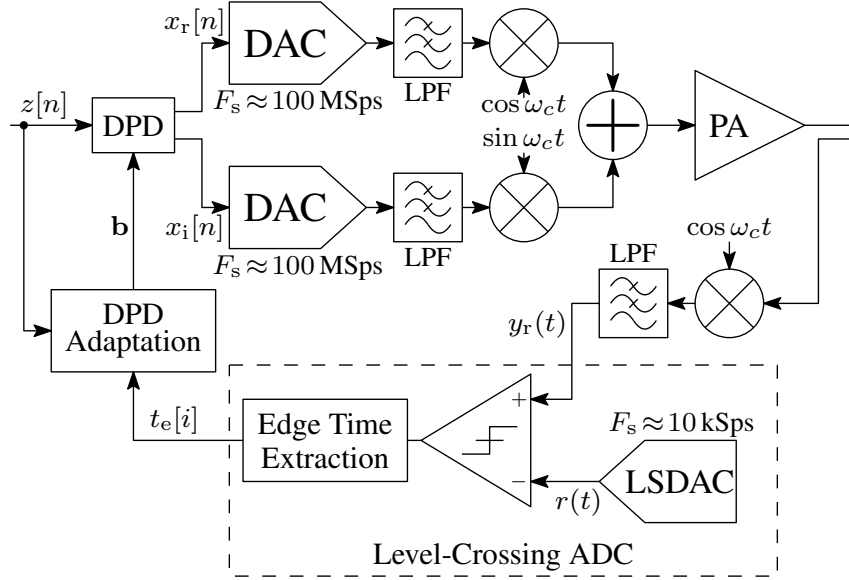

Fig. 5.1: Linearisation of a PA by the DPD with a level-crossing ADC. The edge time extraction circuit provides the time stamps $t_\mathrm{e}[i]$ of edges at the comparator output.

5.2 Basic Principles of DPD with LC-ADC

We can easily rewrite equation (1.2) of the MP model into the continuous-time domain as

$$y(t) = \sum_{k=1}^{K} \sum_{q=0}^{Q} b_{k,q} x(t - qT)|x(t - qT)|^{k-1}. \tag{5.1}$$

The system of equations for solving the PA coefficients consists of N equations. Assuming that signal $x(t)$ is sampled at distinct arbitrary time instants $t_1, t_2, \ldots, t_N$,

we can arrange the system of equations as

$$
\begin{bmatrix} y(t_1) \\ y(t_2) \\ \vdots \\ y(t_N) \end{bmatrix} = \begin{bmatrix} x(t_1) & \dots & x(t_1)|x(t_1)| & x(t_1-T)|x(t_1-T)| & \dots & x(t_1-QT)|x(t_1-QT)|^{K-1} \\ x(t_2) & \dots & x(t_2)|x(t_2)| & x(t_2-T)|x(t_2-T)| & \dots & x(t_2-QT)|x(t_2-QT)|^{K-1} \\ \vdots & \ddots & \vdots & \vdots & \ddots & \vdots \\ x(t_N) & \dots & x(t_N)|x(t_N)| & x(t_N-T)|x(t_N-T)| & \dots & x(t_N-QT)|x(t_N-QT)|^{K-1} \end{bmatrix} \begin{bmatrix} b_{1,0} \\ \vdots \\ b_{2,0} \\ b_{2,1} \\ \vdots \\ b_{K,Q} \end{bmatrix}.
$$

$$(5.2)$$

Considering the DPD feedback with the LC-ADC from Fig. 5.1, the signal $y_\mathrm{r}(t)$ is known only for $t = t_\mathrm{e}[i]$ when the feedback signal equals the set threshold $r(t)$. Time stamps $t_\mathrm{e}[i]$ are the instantaneous times of transitions of signal $y_\mathrm{r}(t)$ over the reference voltage $r(t)$. The equation system can be expressed in the matrix form by arranging the output samples, model coefficients and the basis functions into vectors, i.e.

$$
\boldsymbol{\phi}_{k,q}^{(x)} = \begin{bmatrix} \phi_{k,q}^{(x)}(t_1) & \phi_{k,q}^{(x)}(t_2) & \dots & \phi_{k,q}^{(x)}(t_N) \end{bmatrix}^T,
$$
$$
\boldsymbol{r} = \begin{bmatrix} r(t_1) & r(t_2) & \dots & r(t_N) \end{bmatrix}^T =
$$
$$
= \begin{bmatrix} y_\mathrm{r}(t_1) & y_\mathrm{r}(t_2) & \dots & y_\mathrm{r}(t_N) \end{bmatrix}^T, \qquad (5.3)
$$
$$
\boldsymbol{b} = \begin{bmatrix} b_{1,0} & b_{1,1} & \dots & b_{1,Q} & b_{2,0} & \dots & b_{K,Q} \end{bmatrix}^T,
$$
$$
\boldsymbol{U}_x = \begin{bmatrix} \boldsymbol{\phi}_{1,0}^{(x)} & \boldsymbol{\phi}_{1,1}^{(x)} & \dots & \boldsymbol{\phi}_{1,Q}^{(x)} & \boldsymbol{\phi}_{2,0}^{(x)} & \dots & \boldsymbol{\phi}_{K,Q}^{(x)} \end{bmatrix}.
$$

The LS solution of the PA model coefficients in the matrix form is expressed as

$$
\begin{bmatrix} \boldsymbol{b}_\mathrm{r} \\ \boldsymbol{b}_\mathrm{i} \end{bmatrix} = (\boldsymbol{A}_x^H \boldsymbol{A}_x)^{-1} \boldsymbol{A}_x^H \boldsymbol{r}. \qquad (5.4)
$$

5.3   Measurements

The linearisation performance of the DPD adapted by a comparator in the feedback was evaluated at three distinct setups: narrow-band and high-band setups with a Matlab comparator model and a setup with a real hardware LC-ADC. The wide-band setup (Fig 5.2) provides bandwidth of up to 4096 MHz, but due to its certain imperfections the linearisation performance might be degraded.

The proposed concept was proved on a measurement setup with our custom-designed feedback module with a real hardware LC-ADC. The module contains the comparator, an edge-time extraction circuit, feedback down-converting IQ mixer, and the clock distribution system. The measurement setup and the realised feedback module are captured in photographs in Fig. 5.3.
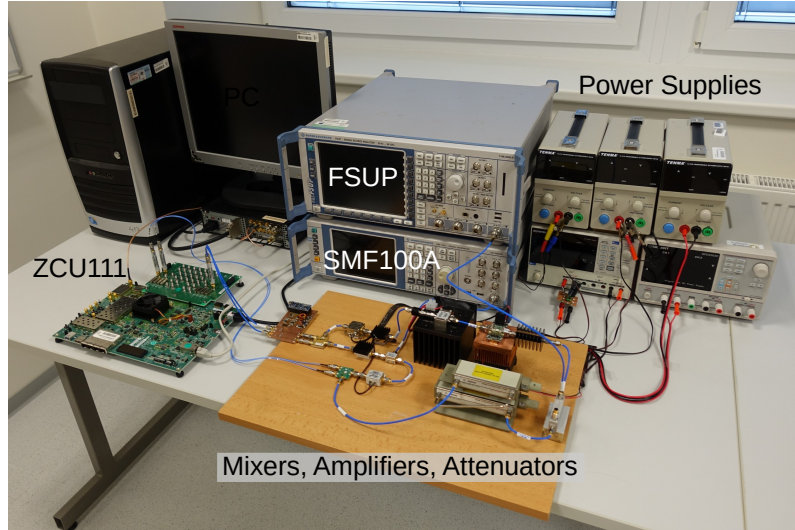
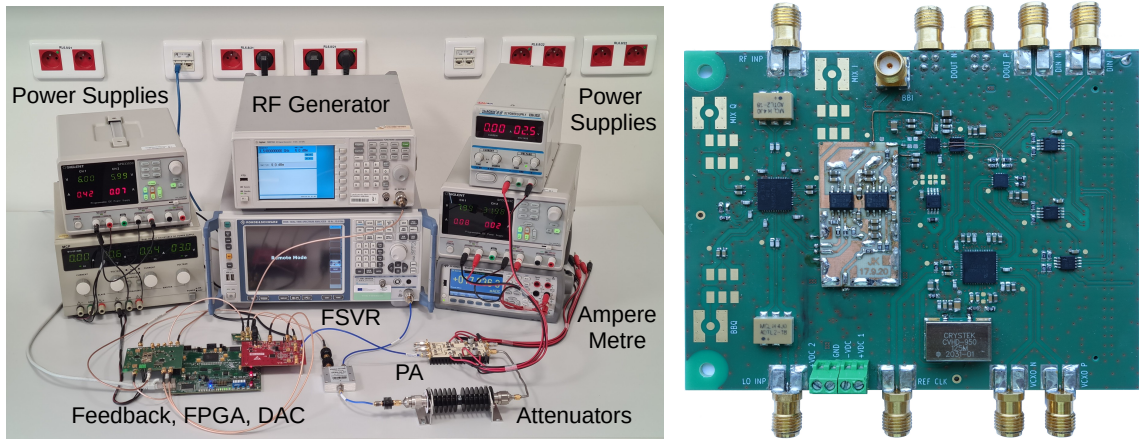Fig. 5.2: Photograph of the wide-band measurement setup.

Fig. 5.3: Photographs of the measurement setup with the hardware LC-ADC and of the realised feedback module.

5.4 Measurement Results

Fig. 5.4a depict the AM/AM characteristics of the PA with the wide-band setup, adapted DPD, and linearised transmitter. The measured *power spectral density* (PSD) for the proposed and conventional DPD compared to the PA output PSD without DPD is shown in Fig. 5.4b. The achieved linearisation performance metrics are summarised in Tab. 5.1. T The proposed adaptation with a comparator in the feedback achieves slightly higher (worse) ACPR and NMSE than the conventional DPD adaptation. Both adaptation methods achieve a similar *error vector magnitude* (EVM) of the transmitted signal.
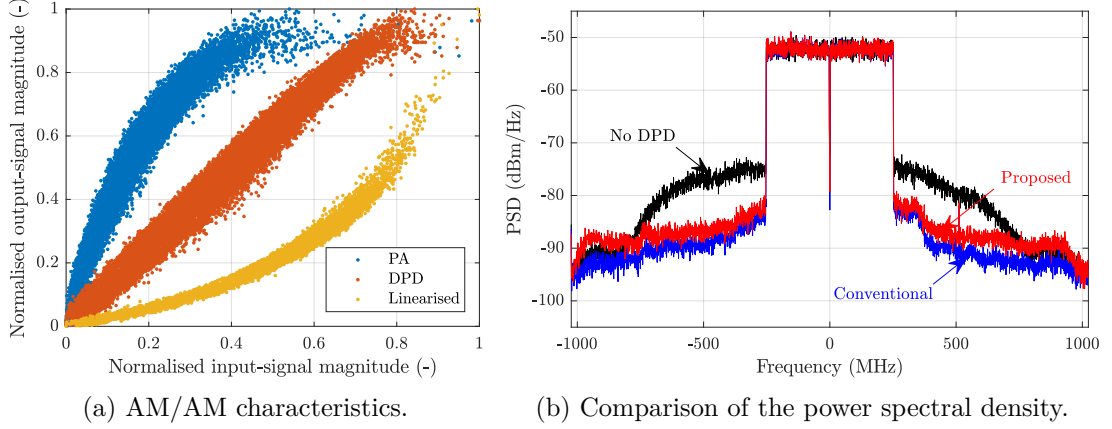
(a) AM/AM characteristics.

(b) Comparison of the power spectral density.

Fig. 5.4: Measurement results for the wide-band setup.

Tab. 5.1: Wide-band measurement results of NMSE, EVM, and ACPR.

	P_{main} (dBm)	NMSE (dB)	EVM (%)	ACPR (dB)
Without DPD	34.8	-17.7	8.31	-26.3
Conventional	34.8	-22.2	5.01	-36.4
LC-ADC	34.9	-21.6	5.23	-34.5

EVM of the generated signal is 1.25% due to the nonorthogonality caused by the inherent F-OFDM filtering.

Fig. 5.6 shows the comparison of the resulting spectra for the conventional DPD and the proposed feedback comparator with the spectrum of the PA output without the linearisation. Fig. 5.5 show the evolution of ACPR in the iterations throughout the measurement. The horizontal black dashed lines depict the individual metrics without the DPD for the same main-channel power.

Tab. 5.2 summarises the DPD linearisation performance. We can observe that the proposed method with the feedback comparator did not achieve the linearisation performance of the conventional method. This could be caused by the limited number of points acquired by the comparator and used for the DPD adaptation. This limitation is, however, the limitation of our setup rather than the limitation of the proposed method.
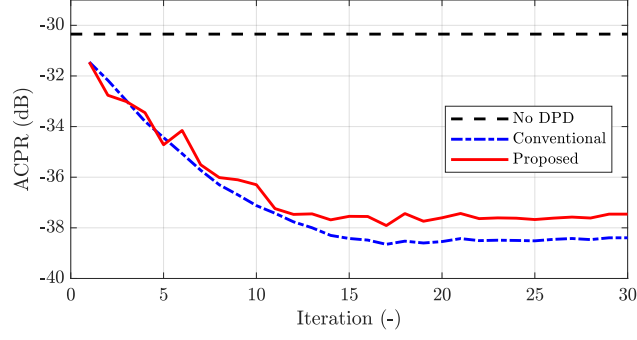
Fig. 5.5: Evolution of the ACPR during the DPD adaptation with the setup with a hardware LC-ADC.
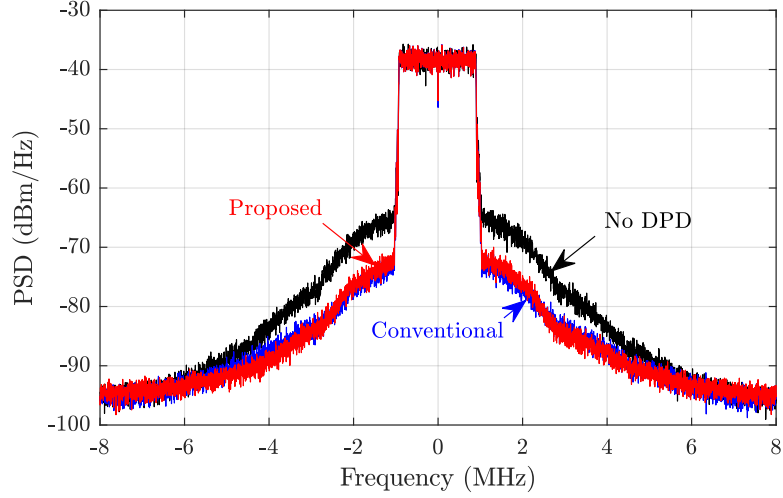
Fig. 5.6: Comparison of the measured power spectral density on the setup with a hardware LC-ADC.

Tab. 5.2: Measurement results of NMSE, EVM, and ACPR for the DPD with the proposed LC-ADC and conventional feedback on the setup with the hardware LC-ADC.

	P_{main} (dBm)	NMSE (dB)	EVM (%)	ACPR (dB)
Without DPD	24.4	-21.9	7.0	-30.4
Conventional	24.3	-27.2	4.9	-38.5
LC-ADC	24.2	-26.0	5.2	-37.6

EVM of the generated signal is 3.1% due to the nonorthogonality caused by the inherent F-OFDM filtering.

5.5 Conclusion

In this chapter, we have proposed a novel method for DPD adaptation with the LC-ADC replacing the conventional ADCs. We have demonstrated the principle of the DPD adaptation with level-crossing detection by a comparator in the feedback. We have shown that the proposed architecture reduces power consumption by approximately 75% compared with the conventional DPD architectures and by approximately 50% compared with the DPD from [4]. The linearisation performance has been evaluated by three measurements, where the proposed DPD achieved comparable linearisation performance to the conventional DPD architectures. We have achieved linearisation of a signal with 500 MHz bandwidth with the wide-band setup with the improvement of 10 dB in ACPR and 3.3% in EVM for the conventional architecture and 8 dB in ACPR and 3.1 % in EVM for the proposed architecture with the LC-ADC. For the last measurement, we designed our feedback module with a real comparator and incorporated it into the measurement setup for the predistortion. Despite all the technical limitations of this setup, the adapted predistorter achieved an improvement of 8 dB in ACPR and 2.1% in EVM for the conventional architecture and 7 dB in ACPR and 1.8% in EVM for the proposed architecture with the designed feedback module.

6 Conclusion

Digital predistortion is considered to be the most advanced and best performing linearisation technique. However, at the same time, it is one of the most complex and computationally demanding techniques. The required extra computational resources and feedback circuits for DPD adaptability represent additional expenses for implementing DPDs and the main limiting factors for their wide spread use across various applications. Although a lot of research has been conducted in this field, there is still plenty of room for improvements in this area. Therefore, we have oriented this thesis toward low-complexity methods for DPD adaptation. The main contributions of this thesis are three key methods to lower the complexity of DPDs:

- real-valued feedback,
- feedback sample selection,
- feedback with an LC-ADC.

The adaptation with real-valued feedback samples enables saving one of two conventionally-employed feedback ADCs. We have shown that the proposed method achieves the same linearisation performance as the conventional approaches and reduces the power consumption and additional expenses on the feedback circuit. The real-valued feedback principle is generally applicable without limitations. Even already realised transmitters with conventional feedback circuits could turn off one feedback ADC, reduce the feedback-circuit power consumption and benefit from improved immunity to feedback IQ imbalances.

The feedback sample selection has been intrinsically based on the undersampling feedback methods. We have shown that only a few feedback samples are required for successful DPD adaptation if the samples are carefully selected. The limited number of required collected samples decreases the size of vectors and matrices entering the calculations and, hence, reduces the computational complexity of DPD adaptation. We have proposed several methods for feedback sample selection, two of them have been driven by respecting a predefined histogram. The proposed histogram-based methods respect both nonlinear PA characteristics and statistical properties of the transmitted signal. In our simulations and measurements, they have achieved the highest reduction of the required number of feedback samples and, consequently, the highest computational complexity reduction. Even the undersampling feedback alone can lead to a significant reduction (≈ 40 times) of the feedback ADC power consumption. The sample selection additionally reduces the computational complexity of DPD adaptation. The performed simulations indicate a 400-time reduction in computation complexity in the number of required multiplications and additions.

The feedback sample selection and undersampling principles are generally applicable and, even more, both principles can be potentially combined with the real-valued feedback principle to reduce even more power consumption and hardware complexity. The feedback sample selection can be applied without any limitations in already-realised transmitters, because its implementation requires only firmware modification. In certain cases, the undersampling could be potentially implemented in already-realised transmitters to reduce the feedback ADC power consumption. To achieve this, the hardware would need to allow for a changing ADC sampling clock frequency. Of course, maximum benefits can be exploited if a new transmitter design is adjusted for all these methods.

The proposed feedback with an LC-ADC replaces a conventional feedback ADC with a simple comparator complemented by a low-speed *digital-to-analogue converter* (DAC). Its real implementation in the hardware requires a different approach for time and amplitude calibrations. For this purpose, we have designed and tested a method based on duty cycle measurements for amplitude calibration which does not require time synchronisation. We have synchronised the time in two steps: first coarsely with sample resolution and later finely with subsample resolution. In both steps, we transmitted an arbitrary signal with edges at different time positions and calculated the signal delay by fitting the transmitted signal with the observed comparator output. In all the conducted measurements, the DPD with LC-ADC adaptation achieved performance similar to that of the conventional DPD. A system comparison example has shown that the proposed LC-ADC feedback can significantly reduce the feedback power consumption ($\approx$ 36 times) or can achieve higher linearisation bandwidth with unchanged power consumption.

The usability of the LC-ADC for DPD adaptation is practically limited to special designs. We expect the LC-ADC could replace conventional ADCs in highly integrated feedback circuits. These integrated designs could benefit from the smaller footprint and lower power consumption of a simple comparator than that of complex high-speed ADCs. Additionally, the presented limitations and required compensations and calibrations could be more easily achievable as the circuit parameters can be better controlled on a chip than in a discrete realisation. The LC-ADC concept, therefore, currently seems to be impractically applicable to designs with discrete feedback circuits and is not suitable for already-realised transmitters, in contrast to the two previously presented methods. Even though the LC-ADC concept is not generally applicable, we demonstrated its funcionality by the first proof-of-concept implementation and we consider it the most advanced and interesting technique presented in this thesis. We believe its main ideas will be employed or improved in the future.

6.1 Potential Future Challenges

Recent review papers [1,2] emphasised the importance of digital predistortion for the 5G or even 6G high-speed wireless communications and identified some potential future challenges. These primarily included improving DPD linearisation performance in general, lowering power consumption demands for DPD linearisation by utilising hybrids of analogue and digital predistorters, effective predistortion for phased array antennas and massive MIMO systems, and increasing linearised bandwidth. In addition, due to our experience, the power consumption of the auxiliary circuits required for the DPD adaptation might be reduced more. One possible approach, which we would like to analyse in the future, is the possibility of avoiding the feedback down-converting mixer which is usually a very power demanding component, especially in wideband applications. Another potential of reducing digital predistortion complexity could be completely avoiding classic feedback and adapting to the PA nonlinearity changes based on a simpler input, e.g. PA temperature. Even though this approach seems to be straightforward, due to our best knowledge, the current state-of-the-art research lacks a comprehensive study of temperature and ageing effects on PA linearity changes and, therefore, it is hard to predict the abilities and performance of simpler DPDs without full adaptability.

Although there are still unanswered questions and many potential challenges to be addressed in the future, we believe that this dissertation thesis satisfies its goal and extends the current state-of-the-art knowledge in the field of digital predistortion aiming at low-complexity methods. We hope this thesis will supplement the published papers and provide a different view on the presented topics and will be one of the starting points for young researchers working on low-complexity digital predistortion.

References

[1] Christian Fager, Thomas Eriksson, Filipe Barradas, Katharina Hausmair, Telmo Cunha, and Jose Carlos Pedro. Linearity and Efficiency in 5G Transmitters: New Techniques for Analyzing Efficiency, Linearity, and Linearization in a 5G Active Antenna Transmitter Context. *IEEE Microwave Magazine*, 20(5):35–49, May 2019. `doi:10.1109/MMM.2019.2898020`.

[2] Andzej Borel, Vaidotas Barzdenas, and Aleksandr Vasjanov. Linearization as a Solution for Power Amplifier Imperfections: A Review of Methods. *Electronics*, 10(9):1073, May 2021. `doi:10.3390/electronics10091073`.

[3] Jessica Chani-Cahuana, Mustafa Özen, Christian Fager, and Thomas Eriksson. Digital Predistortion Parameter Identification for RF Power Amplifiers Using Real-Valued Output Data. *IEEE Transactions on Circuits and Systems II: Express Briefs*, 64(10):1227–1231, Oct. 2017. `doi:10.1109/TCSII.2017.2686004`.

[4] Haoyu Wang, Gang Li, Chongbin Zhou, Wei Tao, Falin Liu, and Anding Zhu. 1-bit Observation for Direct-Learning-Based Digital Predistortion of RF Power Amplifiers. *IEEE Transactions on Microwave Theory and Techniques*, 65(7):2465–2475, Jul. 2017. `doi:10.1109/TMTT.2016.2642945`.

[5] N. Guan, N. Wu, and H. Wang. Digital Predistortion of Wideband Power Amplifier With Single Undersampling ADC. *IEEE Microwave and Wireless Components Letters*, 27(11):1016–1018, Nov. 2017. `doi:10.1109/LMWC.2017.2750059`.

[6] F. M. Ghannouchi and O. Hammi. Behavioral Modeling and Predistortion. *IEEE Microwave Magazine*, 10(7):52–64, Dec. 2009. `doi:10.1109/MMM.2009.934516`.

[7] J. Zhao, Y. Liu, C. Yu, J. Yu, and S. Li. A Modified Band-Limited Digital Predistortion Technique for Broadband Power Amplifiers. *IEEE Communications Letters*, 20(9):1800–1803, Sep. 2016. `doi:10.1109/LCOMM.2016.2585652`.

[8] J. Kim and K. Konstantinou. Digital predistortion of wideband signals based on power amplifier model with memory. *Electronics Letters*, 37(23):1417–1418, Nov. 2001. `doi:10.1049/el:20010940`.

[9] L. Guan and A. Zhu. Simplified Dynamic Deviation Reduction-Based Volterra Model for Doherty Power Amplifiers. In *Workshop on Integrated Nonlinear*

Microwave and Millimetre-Wave Circuits, pages 1–4, Apr. 2011. `doi:10.1109/INMMIC.2011.5773325`.

[10] Z. Yu, H. Xie, and E. Zhu. Wide-band Linear Characteristic Compensation for DPD Systems with Direct Learning. In *Asia-Pacific Microwave Conference Proceedings (APMC)*, pages 790–793, Nov. 2013. `doi:10.1109/APMC.2013.6694933`.

[11] Jessica Chani-Cahuana, Per Niklas Landin, Christian Fager, and Thomas Eriksson. Iterative Learning Control for RF Power Amplifier Linearization. *IEEE Transactions on Microwave Theory and Techniques*, 64(9):2778–2789, Sep. 2016. `doi:10.1109/TMTT.2016.2588483`.

[12] Qian Zhang, Wenhua Chen, and Zhenghe Feng. Reduced Cost Digital Predistortion Only With In-Phase Feedback Signal. *IEEE Microwave and Wireless Components Letters*, 28(3):257–259, Mar. 2018. `doi:10.1109/LMWC.2018.2797541`.

[13] Haoyu Wang, Gang Li, Yikang Zhang, Falin Liu, and Anding Zhu. Forward modeling assisted 1-bit data acquisition based model extraction for digital predistortion of RF power amplifiers. In *IEEE Topical Conference on RF/Microwave Power Amplifiers for Radio and Wireless Applications (PAWR)*, pages 59–62, Jan. 2017. `doi:10.1109/PAWR.2017.7875573`.

[14] Yikang Zhang, Haoyu Wang, Gang Li, and Falin Liu. One-bit in-phase observation for direct learning-based digital predistortion with modified frequency-domain delay estimation and alignment. *International Journal of RF and Microwave Computer-Aided Engineering*, 27(9):e21149, 2017. `doi:10.1002/mmce.21149`.

[15] Pablo Pascual Campo, Vesa Lampu, Lauri Anttila, Alberto Brihuega, Markus Allén, Yan Guo, and Mikko Valkama. Closed-Loop Sign Algorithms for Low-Complexity Digital Predistortion: Methods and Performance. *IEEE Transactions on Microwave Theory and Techniques*, 69(1):1048–1062, Jan. 2021. `doi:10.1109/TMTT.2020.3038316`.

[16] Hai Huang, Patrick Mitran, and Slim Boumaiza. Digital Predistortion Function Synthesis Using Undersampled Feedback Signal. *IEEE Microwave and Wireless Components Letters*, 26(10):855–857, Oct. 2016. `doi:10.1109/LMWC.2016.2605500`.

[17] André Prata, Diogo C. Ribeiro, Pedro Miguel Cruz, Arnaldo S. R. Oliveira, and Nuno Borges Carvalho. RF Subsampling Feedback Loop Technique for

Concurrent Dual-Band PA Linearization. *IEEE Transactions on Microwave Theory and Techniques*, 64(12):4174–4182, Dec. 2016. `doi:10.1109/TMTT.2016.2608893`.

[18] Yue Li, Xiaoyu Wang, and Anding Zhu. Sampling Rate Reduction for Digital Predistortion of Broadband RF Power Amplifiers. *IEEE Transactions on Microwave Theory and Techniques*, 68(3):1054–1064, Mar. 2020. `doi:10.1109/TMTT.2019.2944813`.

[19] D. R. Morgan, Zhengxiang Ma, and Lei Ding. Reducing Measurement Noise Effects in Digital Predistortion of RF Power Amplifiers. In *IEEE International Conference on Communications (ICC)*, volume 4, pages 2436–2439, May 2003. `doi:10.1109/ICC.2003.1204371`.

[20] P. N. Landin, A. E. Mayer, and T. Eriksson. MILA - a noise mitigation technique for RF power amplifier linearization. In *IEEE International Multi-Conference on Systems, Signals Devices (SSD14)*, pages 1–4, Feb. 2014. `doi:10.1109/SSD.2014.6808874`.

[21] Rong Zhu. Gradient-Based Sampling: An Adaptive Importance Sampling for Least-squares. In *Conference on Neural Information Processing Systems (NIPS 2016)*, Dec. 2016.

[22] L. Guan and A. Zhu. Optimized Low-Complexity Implementation of Least Squares Based Model Extraction for Digital Predistortion of RF Power Amplifiers. *IEEE Transactions on Microwave Theory and Techniques*, 60(3):594–603, Mar. 2012. `doi:10.1109/TMTT.2011.2182656`.

[23] Tony F. Chan. Rank Revealing QR Factorizations. *Linear Algebra and its Applications*, 88-89:67 – 82, 1987. `doi:https://doi.org/10.1016/0024-3795(87)90103-0`.

Selection of Author's Bibliography

[A1] Jan Kral, Tomas Gotthans, Roman Marsalek, Lukas Jagla, Michal Harvanek, Martin Pospisil, and Markus Rupp. Digital Predistorter Adaptation with a Level-Crossing Analogue-to-Digital Converter [Submitted]. 2022.

[A2] Jan Kral, Tomas Gotthans, Roman Marsalek, Michal Harvanek, and Markus Rupp. On Feedback Sample Selection Methods Allowing Lightweight Digital Predistorter Adaptation. *IEEE Transactions on Circuits and Systems I: Regular Papers*, 67(6):1976–1988, Jun. 2020. `doi:10.1109/TCSI.2020.2975532`.

[A3] Jan Kral, Tomas Gothans, Roman Marsalek, and Michal Harvanek. Digital Predistorter with Real-Valued Feedback Employing Forward Model Estimation. In *International Conference on Telecommunications (ICT)*, pages 471–475, Jun. 2018. `doi:10.1109/ICT.2018.8464937`.

[A4] Jan Kral, Tomas Gotthans, and Michal Harvanek. Analytical Method of Fractional Sample Period Synchronisation for Digital Predistortion Systems. In *International Conference Radioelektronika (RADIOELEKTRONIKA)*, pages 1–5, Apr. 2017. `doi:10.1109/RADIOELEK.2017.7937603`.

[A5] Jan Kral and Tomas Gothans. Direct Learning Architecture For Digital Predistortion with Real-Valued Feedback. In *Conference STUDENT EEICT 2018*, pages 332–336, 2018.

[A6] Jan Kral and Tomas Gothans. Evaluation of Influence of Anti-Aliasing and Reconstruction Filters on Digital Predistortion. In *Conference STUDENT EEICT 2017*, pages 405–409, 2017.

[A7] Michal Harvanek, Roman Marsalek, Jan Kral, Tomas Gotthans, Jiri Blumenstein, Martin Pospisil, and Markus Rupp. Adjacent Channel Interference Cancellation in FDM Transmissions. *IEEE Transactions on Circuits and Systems I: Regular Papers*, 67(12):5417–5428, Dec. 2020. `doi:10.1109/TCSI.2020.2995350`.

[A8] Tomáš Götthans, Roman Maršálek, Jan Král, and Tomáš Urbanec. Linearity and Efficiency Enhancement Techniques for Satellite Communications. In *IEEE Topical Conference on RF/Microwave Power Amplifiers for Radio and Wireless Applications (PAWR)*, pages 54–57, Jan. 2022. `doi:10.1109/PAWR53092.2022.9719692`.